

# LONGITUDINAL BEAM DYNAMICS WITH A HIGHER-HARMONIC CAVITY FOR BUNCH LENGTHENING\*

G. Bassi<sup>†</sup>, J. Tagger, Brookhaven National Laboratory, Upton, 11973 NY, USA

## Abstract

We discuss the longitudinal beam dynamics in storage rings in the presence of a higher-harmonic cavity (HHC) system for bunch lengthening. We first review the general conditions for HHC operations, either in active or passive mode, assuming the stability of the system. For uniform filling patterns, a distinction is made between operations with a normal-conducting HHC, where optimal conditions for bunch lengthening can be satisfied, and operations with super-conducting HHC, where optimal conditions can be met only approximately. The option to operate the NSLS-II storage ring with a passive, super-conducting third harmonic cavity (3HC) system is discussed next. The stability and performance of the system in the presence of a gap in the uniform filling, which corresponds to the present mode of operation of the NSLS-II storage ring, is investigated with self-consistent Vlasov-Fokker-Planck simulations performed with the code SPACE [1].

## INTRODUCTION

Higher-harmonic cavities (HHCs) play a crucial role for stable operations of present and future low-emittance storage rings. The primary benefic effect provided by the HHC is bunch lengthening without energy spread increase, with consequent beam lifetime improvement and reduction of the effect of intrabeam scattering on the transverse emittance [2]. Besides bunch lengthening, the highly nonlinear potential well distortion produced by the HHC introduces a strong dependence of the synchrotron tune on the amplitude of synchrotron oscillations. The induced anharmonic motion with enhanced synchrotron tune spread provides a powerful mechanism, known as Landau damping, for the suppression of collective instabilities. Moreover, the increase in bunch length and synchrotron tune spread can enhance the stabilizing effect of positive chromaticity on the transverse oscillations and help to stabilize higher-order head-tail modes [2]. The option considered for the NSLS-II storage ring is to operate with a passive superconducting 3HC [3, 4], a choice motivated by the successful development and operation of the superconducting 3HC system at the ELETTRA [5] and SLS [6] storage rings, a system that has been developed in the framework of the SUPER-3HC project [7]. The SUPER-3HC project represented the first superconducting application of a HHC system in storage rings, taking advantage of the very high quality factor of the superconducting cavity and the associated narrow bandwidth, allowing for the tuning of the 3HC very near to the

third harmonic of the beam, without exciting longitudinal instabilities [5]. The success of the 3HC operation at the ELETTRA storage ring is substantiated by a beam lifetime improvement by more than a factor of three with respect to the nominal value, an improvement that has led to a change in the refilling frequency of the storage ring, allowing a refilling every 48 hr instead of every 24 hr, with benefit for the reliability and stability of user's operations and relevant benefit even for the machine thermal stability [5]. The success with the operation of a 3HC at the SLS storage ring is substantiated by a bunch lengthening up to a factor of three and a beam lifetime increase greater than a factor of two, achieved with stable conditions at the design current of 400 mA [6]. The success experienced at the ELETTRA and SLS storage rings has clearly shown that the very high quality factor of the superconducting HHC renders the performance of the HHC system less sensitive to high-order modes (HOMs) driven longitudinal coupled bunch instabilities, which is a major issue with normal conducting HHCs, where powerful longitudinal feedback systems are often needed for stable operations. Performance limiting factors, however, such as transients effects induced by non uniform filling patterns and the beam phase instability [8], can be detrimental for stable HHC operations, and need to be carefully investigated with detailed design studies. Accurate numerical simulations represent an essential part of the aforementioned design studies, with their goal to determine feasible conditions of operation and their range of applicability. To this end, the stability and performance of the passive superconducting 3HC system for the NSLS-II storage ring is studied numerically with the parallel, particle tracking code SPACE [1], which allows to follow self-consistently the dynamics of  $h$  bunches, where  $h$  is the number of RF buckets, in arbitrary multi-bunch configurations. The specific goal of the numerical simulations is to determine stable HHC cavity settings and to study the performance limitation due to a gap in the uniform filling, which represents the nominal NSLS-II mode of operation.

## OPERATIONS WITH HIGHER-HARMONIC CAVITIES

In the discussion of the theoretical conditions for optimal bunch lengthening, we assume a stable, beam loading compensated HHC system characterized by an equilibrium multi-bunch configuration. Radiation damping and quantum fluctuations are excluded from the analysis. The overall stability of the HHC system, including radiation damping and quantum fluctuations, together with the inclusion of a model for beam loading compensation, will be addressed in the next section with time-dependent Vlasov-Fokker-Planck simulations.

\* Work supported by Brookhaven Science Associates, LLC under Contract No. DE-AC02-98CH10886 with the U.S. Department of Energy

<sup>†</sup> gbassi@bnl.gov

## Active Higher-Harmonic Cavity

We assume that the voltage  $V(\tau)$  seen by a particle in the beam with arrival time  $\tau$  is

$$V(\tau) = V_{rf}[\sin(\omega_{rf}\tau + \phi_s) - r \sin(m\omega_{rf}\tau + \phi_m)] - \frac{U_s}{e} \\ =: V_c(\tau) - \frac{U_s}{e}, \quad (1)$$

where  $V_{rf}$  is the amplitude of the voltage of the main rf cavity,  $\omega_{rf} = h\omega_0$ , where  $h$  is harmonic number and  $\omega_0$  the angular revolution frequency,  $m$  is the order of the HHC and  $r$  the ratio of HHC to main cavity amplitude voltage,  $U_s$  energy loss per turn,  $e$  the electron charge,  $\phi_s$  and  $\phi_m$  the phases of the synchronous particle in the main and HHC respectively. Here  $V_c(\tau)$  is the total rf voltage produced by the main rf cavity and by HHC.

The longitudinal dynamics in the double RF system described by Eq. (1) has been comprehensively discussed, together with optimal conditions for bunch lengthening, by Hofmann and S. Myers in 1980 [9]. See also [10]. Here we summarize the main results.

Table 1: NSLSII Parameters

Parameter	Symbol	Value	Unit
Energy reference particle	$E_0$	3	GeV
Average current	$I_0$	500	mA
Gap in the uniform filling	$g$	260	
Harmonic number	$h$	1320	
Circumference	$C$	792	m
Bunch duration	$\sigma_\tau$	14.5	ps
Energy spread	$\sigma_p$	0.00087	
Energy loss per turn	$U_s$	674	keV
Momentum compaction	$\alpha$	0.00037	
Revolution frequency	$f_0$	378.5	kHz

Table 2: RF Parameters Main (2 Cavities) and 3HC (1 Cavity)

Per Cavity Parameters	Symbol	Value	Unit
main frequency	$\omega_{rf}$	$2\pi \times 499.68$	MHz
HHC frequency	$3\omega_{rf}$	$2\pi \times 1499.04$	MHz
main voltage	$V_{rf}$	1.7	MV
main shunt impedance	$R_M$	2.97	MΩ
main quality factor	$Q_M$	66817	
HHC shunt impedance	$R_H$	22880	MΩ
HHC quality factor	$Q_H$	$2.6 \times 10^8$	

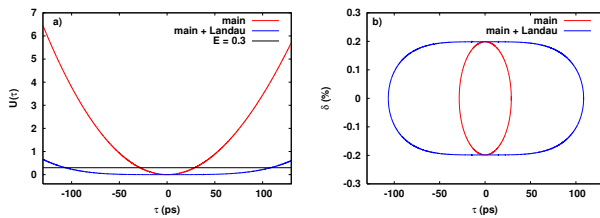


Figure 1: a) Potential energy  $U(\tau)$  without HHC (red line) and with HHC (blue line) with parameters of the NSLS-II storage ring (see Table 1) satisfying Eq. (5-7). b) Phase space portrait corresponding to a) for  $E = 0.3$ .

To compensate for the energy loss  $U_s$ , we require that the voltage seen by the synchronous particle is zero, i.e.  $V(0) = 0$ . In addition, we require  $V'(0) = V''(0) = 0$ , where  $' = d/d\tau$ . Thus

$$\sin \phi_s = r \sin \phi_m + \frac{U_s}{eV_{rf}}, \quad (2)$$

$$\cos \phi_s = rm \cos \phi_m, \quad (3)$$

$$\sin \phi_s = rm^2 \sin \phi_m, \quad (4)$$

which, solved for  $\phi_s$ ,  $\phi_m$  and  $r$  give

$$\sin \phi_s = \frac{m^2}{m^2 - 1} \sin \phi_{s0}, \quad \sin \phi_{s0} = \frac{U_s}{eV_{rf}}, \quad (5)$$

$$\tan \phi_m = \frac{m \sin \phi_{s0}}{\sqrt{(m^2 - 1)^2 - m^4 \sin^2 \phi_{s0}}}, \quad (6)$$

$$r = \frac{1}{m} \sqrt{1 - \frac{m^2}{m^2 - 1} \sin^2 \phi_{s0}}. \quad (7)$$

where we introduced  $\phi_{s0}$ , the synchronous phase in absence of the HHC. With the voltage given by Eq. (1), from the Hamiltonian

$$H(\tau, \delta) = \frac{\eta}{2} \delta^2 + U(\tau),$$

$$U(\tau) = \frac{eV_{rf}}{E_0 T_0 \omega_{rf}} \left[ \cos(\omega_{rf}\tau + \phi_s) - \cos \phi_s + \frac{r}{m} \cos \phi_m \right. \\ \left. - \frac{r}{m} \cos(m\omega_{rf}\tau + \phi_m) + \omega_{rf}\tau \sin \phi_{s0} \right], \quad (8)$$

follow the longitudinal equations of motion

$$\dot{\tau} = \frac{\partial H}{\partial \delta} = \eta \delta,$$

$$\dot{\delta} = -\frac{\partial H}{\partial \tau} = \frac{eV_{rf}}{E_0 T_0} \left[ \sin(\omega_{rf}\tau + \phi_s) - r \sin(m\omega_{rf}\tau + \phi_m) \right. \\ \left. - \sin \phi_{s0} \right], \quad (9)$$

where  $' = d/dt$ ,  $\eta = \alpha - \gamma_0^{-2}$  is the slippage factor, where  $\gamma_0$  is the Lorentz factor,  $\delta = (E - E_0)/E_0$  is the relative energy deviation with respect to the synchronous particle with energy  $E_0$ , and the arbitrary constant in the definition of  $U(\tau)$  has been chosen in order to satisfy  $U(0) = 0$ . Since  $U$  does not depend explicitly on time,  $H$  is a constant of motion and setting  $E = H$  we have  $\delta(\tau) = \pm \sqrt{2(E - U(\tau))/\eta}$ ,  $E = \text{const.}$  In Fig. 1a we show the potential energy  $U(\tau)$  with only the main rf cavity (red line) and with a third-harmonic cavity (blue line) with parameters satisfying Eqs. (5-7) for the NSLS-II storage ring (see Table 1). In Fig. 1b we show the corresponding phase space portrait for  $E = 0.3$ . The optimal conditions satisfied by the voltage  $V(\tau)$  induce a bunch lengthening without an increase of the energy spread. According to Table 1,  $r = 0.329 \approx 1/3$ , thus the peak voltage induced by the harmonic cavity system is roughly one third the peak voltage  $V_{rf}$  of the main cavity system. In the case of no energy loss ( $U_s = 0$ ) the conditions (2)-(4) simplify to  $\phi_s = \phi_m = 0$  and  $r = 1/m$ . In Fig.2a we plot the

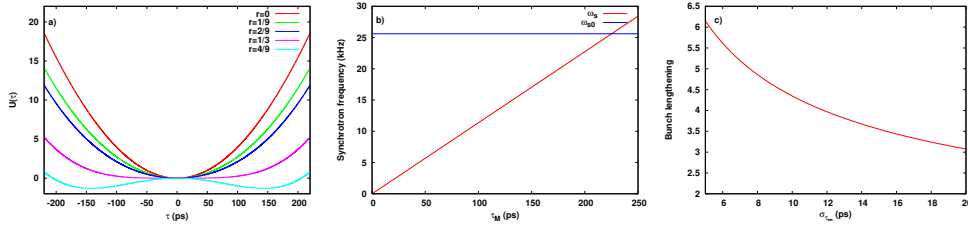


Figure 2: a) Potential energy  $U(\tau)$  in the active case ( $m = 3$ ) and for no energy loss ( $U_s = 0$ ). b) Synchrotron frequency  $\omega_s$  for the quartic potential (red line) and synchrotron frequency  $\omega_{s0}$  for the quadratic potential (blue line). c) Bunch lengthening  $u$  vs. bunch length  $\sigma_{\tau_m}$  (w/o HHC).

potential energy  $U(\tau)$  for  $m = 3$  and different values of  $r$ . For  $r = 4/9$  the potential energy has two stable fixed points close to  $\pm 150$  ps.

**Small Oscillations** For small oscillations ( $\tau \ll 1$ ) the potential energy  $U(\tau)$  without HHC can be approximated by a quadratic function of  $\tau$

$$U(\tau) = -\frac{eV_{rf}\omega_{rf}\cos\phi_{s0}}{2E_0T_0}\tau^2 =: \frac{\omega_{s0}^2}{2\eta}\tau^2, \quad (10)$$

while with the addition of the harmonic cavity the potential given by Eq.(8) can be approximated by a quartic

$$U(\tau) = -\frac{eV_{rf}(m^2 - 1)\omega_{rf}^3\cos\phi_s}{24E_0T_0}\tau^4. \quad (11)$$

For a potential energy satisfying  $U(-\tau) = U(\tau)$  and  $U(\tau) > 0$  for  $\tau > 0$ , the trajectory is confined in the region  $[-\tau_M, \tau_M] \times [-\delta_M, \delta_M]$  where  $\tau_M$  and  $\delta_M$  satisfy  $U(\tau_M) = E$  and  $\eta\delta_M^2/2 = E$  respectively, thus the amplitude of the trajectory is  $d = 2\tau_M$ . It can be shown that the synchrotron frequency  $\omega_s$  for the quartic potential (11) reads

$$\omega_s(\tau_M) = \frac{\pi}{2}\sqrt{\frac{m^2 - 1}{6}}\sqrt{\frac{\cos\phi_s}{\cos\phi_{s0}}}\frac{\omega_{rf}\omega_{s0}}{K(1/\sqrt{2})}\tau_M, \quad (12)$$

where  $K$  is the complete integral of the first kind. The dependence of the synchrotron frequency on  $\tau_M$  provides Landau damping for beam stability. In Fig. 2b we plot  $\omega_s$  as a function of  $\tau_M$ . It can also be shown that the bunch lengthening factor  $u$  for an equilibrium distribution  $\rho_e$  in the quartic potential (11) reads

$$u := \frac{\sigma_{\tau L}}{\sigma_{\tau m}} = \sqrt{\frac{\Gamma(3/4)}{\Gamma(1/4)}}\left(\frac{24\cos\phi_{s0}}{(m^2 - 1)\omega_{rf}^2\cos\phi_s}\right)^{1/4}\frac{1}{\sqrt{\sigma_{\tau m}}}, \quad (13)$$

where  $\Gamma$  is the Gamma function,  $\sigma_{\tau m} = \eta\sigma_\delta/\omega_{s0}$  is the equilibrium bunch length with only the main cavity, and  $\sigma_{\tau L}$  is the equilibrium bunch length with the harmonic cavity. The bunch lengthening factor  $u$  as a function of  $\sigma_{\tau m}$  is plotted in Fig. 2c. With NSLS-II parameters ( $\sigma_{\tau m} = \sigma_\tau$ ) the bunch lengthening factor reads  $u = 3.7$ .

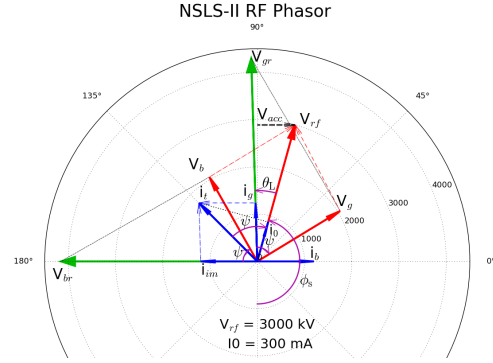


Figure 3: RF phasor of the NSLS-II storage ring during operations with a stored beam current  $I_0 = 300$ mA,  $V_{rf} = 3$  MV,  $\phi_s = 164.5^\circ$ ,  $\theta_L = -17^\circ$ ,  $V_b = 2062$  kV,  $V_g = 2132$  kV and detuning angle  $\psi = 60^\circ$ .

### Passive Higher-Harmonic Cavity

For passive HHC operations, the total RF voltage is given by the sum of the voltage produced by the powered main cavity and the beam voltage induced by the beam in both cavities. We assume in this section that the main cavity is beam loading compensated.

**Operations with Normal-Conducting Cavities.** In the case of stationary bunches uniformly distributed around the ring, and for a narrow-band resonator wake with frequency  $\omega_r$ , shunt impedance  $R_s$  and quality factor  $Q$ , the voltage acting on the beam reads

$$V_C(\tau) = V_{rf}\sin(\phi_s + \omega_{rf}\tau) - i_m R_s \cos\psi \cos(\psi + m\omega_{rf}\tau), \quad (14)$$

where  $i_{im} = 2I_0\tilde{\rho}(\omega)$  and the detuning angle  $\psi$  satisfies

$$\tan\psi = 2Q\delta, \delta = \frac{1}{2}\left(\frac{\omega_r}{m\omega_{rf}} - \frac{m\omega_{rf}}{\omega_r}\right) \approx \frac{\omega_r - m\omega_{rf}}{m\omega_{rf}}. \quad (15)$$

Here  $\tilde{\rho}(\omega)$  is the Fourier transform of the bunch density  $\rho(\tau)$  satisfying  $\rho(-\tau) = \rho(\tau)$ . For Gaussian bunches  $i_{im} = 2I_0e^{-\frac{1}{2}(m\omega_{rf}\sigma_\tau)^2}$ . Imposing the same the conditions (2–4) for the active HHC, by comparing Eq. (1) and Eq. (14) it follows ( $0 < \phi_s < \pi \implies 0 < \psi < \pi/2 \implies \cos\psi > 0$ )

$$\tan\psi = -\cot\phi_m = -m\cot\phi_s, \quad (16)$$

$$R_s = \frac{rV_{rf}}{i_{im}\cos\psi} = \frac{V_{rf}\sin\phi_s}{i_{im}m^2\cos^2\psi}, \quad (17)$$

where we used  $\sin \phi_m = \cos \psi$  ( $\tan \psi = -\cot \phi_m \implies \psi = \phi_m - \pi/2 \implies \sin \phi_m = \cos \psi$ ). Therefore the conditions for passive HHC operations corresponding to the active case (5–7) are

$$\sin \phi_s = \frac{m^2}{m^2 - 1} \sin \phi_{s0}, \quad (18)$$

$$\tan \psi = -\frac{\sqrt{(m^2 - 1)^2 - m^4 \sin^2 \phi_{s0}}}{m \sin \phi_{s0}}, \quad (19)$$

$$R_s = \frac{V_{rf}(m^2 - 1)(1 - \sin \phi_{s0})}{i_{im} m^2 \sin \phi_{s0}}. \quad (20)$$

An important difference to active case is that  $R_s$  is uniquely determined and a function of the beam current  $I_0$ . Notice, however, that these conditions do not impose any constraint on the value of  $Q$ , therefore do not determine uniquely the detuning frequency  $\Delta\omega = \omega_r - m\omega_{rf}$ . The optimal parameters for passive HHC operations of the NSLS-II storage ring according to Tables 1 and 2 are therefore  $\sin \phi_s = 0.4592$ ,  $\tan \psi = 5.8 \implies \psi = 80.22^\circ$  and  $R_s = 9.02 \text{ M}\Omega$ .

**Operations with Super-Conducting Cavities.** According to Table 2, the shunt impedance of the HHC is  $R_H = 22880 \text{ M}\Omega$ , much bigger than the optimal value  $R_s = 9.02 \text{ M}\Omega$ , so the optimal conditions for passive operations can not be met. Good conditions, however, can be found by comparing Eq. (1) and Eq. (14) at  $\tau = 0$ , which gives  $R_s = rV_{rf}/(i_{im} \cos \psi)$ , and by noticing from Eq. (7) that  $r \approx 1/m$ , since to good approximation  $\sin \phi_{s0}^2 \ll 1$ . We therefore impose on the detuning angle  $\psi$  the condition  $\cos \psi = V_{rf}/(mi_{im}R_H)$ , which implies that the detuning frequency  $\Delta\omega_H$  approximately satisfies

$$\Delta\omega_H = \frac{m^2\omega_{rf}i_bR_HV_{rf}}{2Q_HV_{rf}}, \quad (21)$$

where we used Eq. (15) and the fact that  $\sin \psi \ll 1$ . With parameters listed in Table 2, it follows that  $\Delta\omega_H = 2\pi \times 58.24 \text{ kHz}$ .

## NUMERICAL SIMULATIONS

With the inclusion of a model for beam loading compensation, time dependent simulations of the Vlasov-Fokker-Planck equation allow for the study of the overall stability of the HHC system. Moreover, numerical simulations allow for the study of transient effects induced by arbitrary multi-bunch configurations, such as a gap in the uniform filling pattern for ion clearing, which corresponds to the nominal configuration of the NSLS-II storage ring. The numerical simulations of the Vlasov-Fokker-Planck equation discussed in this paper are done with the parallel code SPACE, a particle tracking code that allows for the simultaneous study of short- and long-range wakefield effects in storage rings. The general strategy adopted by SPACE to study multibunch effects is to distribute each bunch to one processor, each with  $\mathcal{N}$  simulations particles representing the bunch population, thus performing the short- and long-range wakefield

calculation in serial and parallel respectively. For more details on the code SPACE see [1]. For steady state beam loading compensation, the algorithm implemented in SPACE is based on the standard phasor diagram, shown in Fig. 3 with parameters of one of the operational settings of the NSLS-II storage ring. The numerical simulations discussed in this paper have been done on the supercomputers Cori and Edison at NERSC [11]. The equations of motion for bunch  $n$  ( $n = 0, \dots, h - 1$ ), shown here without radiation damping and quantum fluctuations, for the general NSLS-II operations with two main cavities and one HC read

$$\begin{aligned} \dot{\tau} &= \eta\delta, \\ \dot{\delta} &= \frac{e}{E_0T_0} \left[ \sum_{i=1}^2 V_{gr,i} \cos \psi_i \sin(\omega_{rf}\tau + \phi_s - \theta_{L,i} + \psi_i) \right. \\ &\quad \left. - V_n(\tau, s) - \frac{U_s}{e} \right], \end{aligned} \quad (22)$$

where  $V_{gr,i}$ ,  $\psi_i$  and  $\theta_{L,i}$  ( $i = 1, 2$ ) correspond to the generator voltage, detuning angle and load angle of the two main cavities respectively, and  $V_n(\tau, s)$  is the total beam loading voltage acting on bunch  $n$ . The numerical simulations discussed in this paper assume the two main cavities with same beam loading parameters, which correspond to the standard mode of operation of the NSLS-II storage ring. By projecting the current phasors shown in Fig. 3 along and perpendicular to the RF voltage phasor,  $V_{gr}$  and  $\psi$  satisfy

$$\tan \psi = \left( 1 + \frac{i_{im,M}}{i_0} \sin \phi_s \right) \tan \theta_L + \frac{i_{im,M}}{i_0} \cos \phi_s, \quad (23)$$

$$V_{gr} = \frac{V_{rf}}{\cos \theta_L} \left( 1 + \frac{i_{im,M}}{i_0} \sin \phi_s \right). \quad (24)$$

where  $i_{im,M} = 2I_0\tilde{\rho}(\omega_{rf})$  is the image current in the main cavity, and  $i_0 = V_{rf}/R_M$ . In the analysis of the performance of the NSLS-II HHC system, we study first the case with a uniform filling pattern, and compare the results with the nominal case, which corresponds to a gap of 260 bunches, (80% fractional filling), and with the case with a gap of 130 bunches (90% fractional filling). In the discussion that follows we omit the subscript  $H$  to label the detuning frequency of the HHC.

### Uniform Fillings

In Fig. 4 we show numerical simulations for values of the HHC detuning frequency  $\Delta f = 45 \text{ kHz}$ ,  $55 \text{ kHz}$  and  $65 \text{ kHz}$ , above and below the value  $\Delta f = 58.24 \text{ kHz}$  calculated in Sect. II for good bunch lengthening conditions. The longitudinal density of the bunches after 100,000 turns is shown in Fig. 4a for  $\Delta f = 45 \text{ kHz}$ , in Fig. 4b for  $\Delta f = 55 \text{ kHz}$  and Fig. 4c for  $\Delta f = 65 \text{ kHz}$ . The bunch lengthening is uniform across the bunch train for  $\Delta f = 55 \text{ kHz}$  and  $\Delta f = 65 \text{ kHz}$ , with values  $\sigma_\tau = 50 \text{ ps}$  and  $\sigma_\tau = 36 \text{ ps}$  respectively, as shown in Fig. 4e and Fig. 4f, corresponding to the bunch lengthening factors  $u = 3.45$  and  $u = 2.48$ . For  $\Delta f = 45 \text{ kHz}$ , the longitudinal density of the bunches shows a double peaked structure and a non-uniform bunch

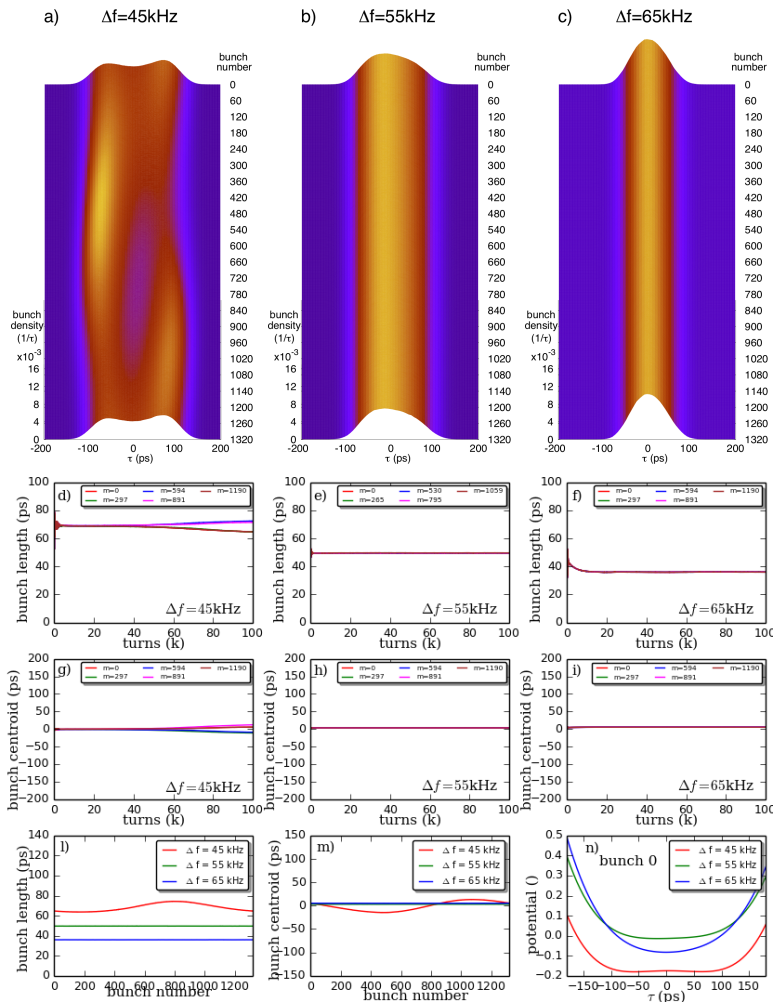


Figure 4: Numerical simulations in the case of uniform filling with detuning frequency  $\Delta f = 45$  kHz, 55 kHz and 65 kHz.

lengthening, as shown in Fig. 4a, Fig. 4g and Fig. 4l. Long term simulations up to 500,000 turns, as plotted in Fig. 4a and Fig. 4g, show that for  $\Delta f = 45$  kHz the HHC system is weakly unstable, signing the transition to an “overstretching” regime, with average bunch length across the train of  $\approx 70$  ps. The potential well of bunch  $n = 0$ , showing two local minima, is shown by the red trace in Fig. 4n.

### Gap in the Uniform Filling: $g = 130$ and $g = 260$

The case of a gap in the uniform filling corresponds to a train of  $M = h - g$  bunches, where  $h$  is the harmonic number and  $g$  is the gap. The case with nominal gap,  $g = 260$ , corresponding to a 80% fractional filling, is compared with the case  $g = 130$ , corresponding to a 90% fractional filling. The main effect introduced by a gap in the uniform filling is a monotonic variation of the bunch centroid across the train, and a reduced, non uniform bunch lengthening. Fig. 5 and Fig. 6 show numerical simulations up to 100,000 turns with gaps  $g = 130$  and  $g = 260$  respectively, for the same HHC detuning frequencies of the uniform case. The monotonic variation of the bunch centroid across the train is evident from the longitudinal density of the bunches

shown in Fig. 5a-c, from the time evolution of the bunch centroids shown in Fig. 5g-i, and from Fig. 5m, where it can be noticed that the range of variation of the bunch centroids increases with the decrease of the HHC detuning frequency. Fig. 5d-f and Fig. 5l show the non uniform bunch lengthening across the train, with a similar average value  $\langle \sigma_\tau \rangle \approx 35$  ps for the different detuning frequencies. We notice that for  $\Delta f = 45$  kHz the bunches in the center of the train have longer bunch length than the bunches in the periphery of the train. The case of nominal gap,  $g = 260$ , is discussed in Fig. 6. A detuning frequency threshold is observed in this case. For detuning frequencies above the threshold, as shown for  $\Delta f = 65$  kHz in Fig. 6c, Fig. 6f and Fig. 6l a stable equilibrium is reached after 100,000 turns, with average bunch length across the train  $\langle \sigma_\tau \rangle \approx 27$  ps, while for detuning frequencies below threshold, as shown in Fig. 6a, Fig. 6d for  $\Delta f = 45$  kHz and Fig. 6b, Fig. 6e and Fig. 6h for  $\Delta f = 55$  kHz, an unstable regime with saturation is observed, with both the bunch lengths and bunch centroids exhibiting a well defined mode of oscillation. The numerical simulations discussed so far have been done with load angle  $\theta_L = 0$ . In the attempt to improve stability, the two unstable

Content from this work may be used under the terms of the CC BY 3.0 licence under the terms of the CC BY 3.0 licence (© 2018). Any distribution of this work must maintain attribution to the author(s), title of the work, publisher, and DOI.

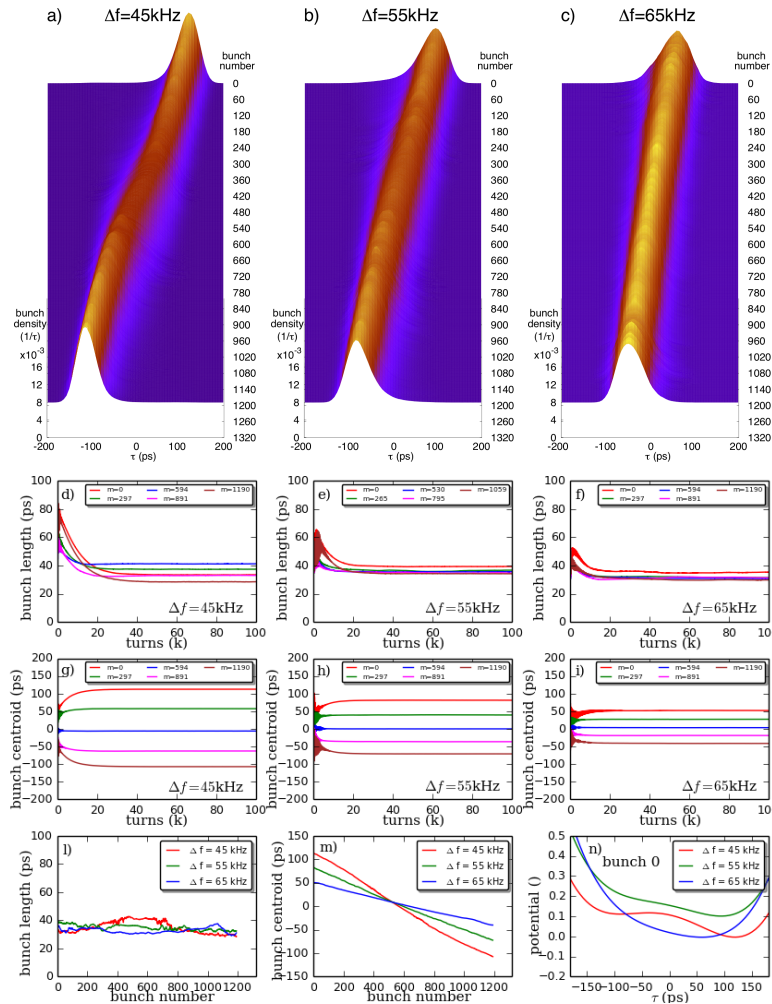


Figure 5: Numerical simulations up to 100,000 turns with a gap  $g = 130$ . HHC detuning frequencies as in Fig. 4.

configurations at the nominal gap  $g = 260$  for  $\Delta f = 45$  kHz and 55 kHz have been simulated with  $\theta_L < 0$ . In both cases the numerical results show that the introduction of a negative load angle is partially effective in stabilizing the HHC system, with the “stabilizing” load angle in the range  $[-20^\circ, 0^\circ]$  for  $\Delta f = 45$  kHz, and  $[-40^\circ, -20^\circ]$  for  $\Delta f = 55$  kHz.

## CONCLUSION

The numerical result clearly show a reduction in both performance and stability of the HHC system with the increase of the gap in the uniform filling, with the case of a gap  $g = 130$ , corresponding to a 90% fractional filling, stable at all the detuning frequencies considered. On the other hand, the nominal case with  $g = 260$ , corresponding to a 80% fractional filling, has shown to be unstable for some values of the detuning frequencies. Moreover, the case with  $g = 130$  has shown a superior performance in terms of bunch lengthening with respect to the nominal case. The performance of stable HHC settings for the nominal case  $g = 260$  and the case  $g = 130$ , as a function of detuning frequency  $\Delta f$  and load angle  $\theta_L$ , is shown in Fig. 7, both in terms of average bunch lengthening and uniformity of the bunch centroid and bunch

length across the train. The average bunch lengthening factor for the 80% and 90% fractional filling is approximately 2 and 2.5 respectively, to be compared with the bunch lengthening factor of the uniform filling case, which, according to Fig. 4g, is approximately 3.5 for  $\Delta = 55$  kHz. The performance reduction in the average bunch lengthening due to a gap in the uniform filling is therefore 45% for  $g = 260$  and 30% for  $g = 130$ . Machine studies are planned at the NSLS-II storage ring to revisit the need of the nominal 80% fractional filling pattern for ion clearing, with the goal to increase the fractional filling towards a more uniform filling pattern. Arbitrary, more general multibunch configurations, such as filling patterns with multiple, smaller gaps than the nominal, are also under consideration. To this end, an analytical calculation to determine the beam loading voltage induced by arbitrary, stationary bunches has been done and implemented in a numerical code for fast parametric scans and guidance in Vlasov-Fokker-Planck simulations of the HHC system [12].

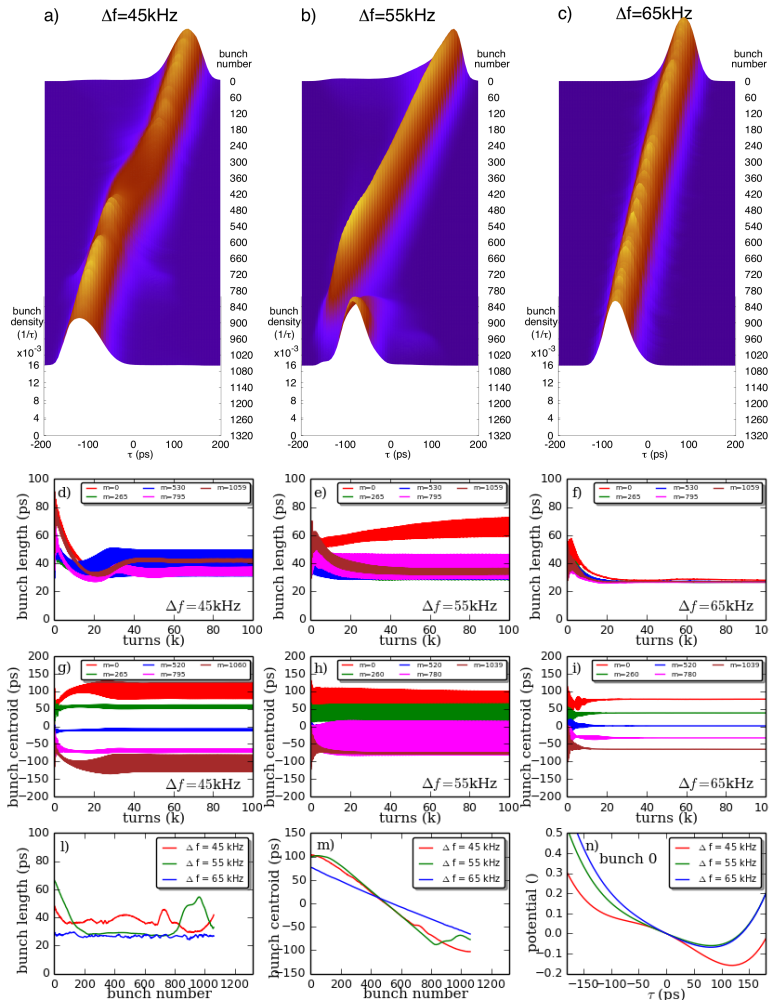


Figure 6: Numerical simulations up to 100,000 turns with nominal gap  $g = 260$ . HHC detuning frequencies as in Fig. 4.

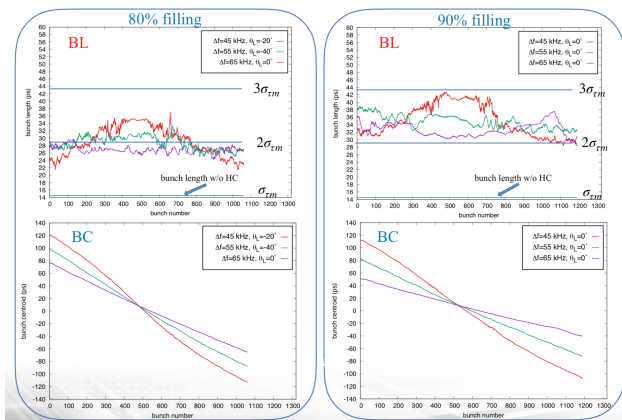


Figure 7: Performance of the HHC stable settings as a function of the detuning frequency  $\Delta$  and load angle  $\theta_L$  for  $g = 260$  (80% fractional filling) and  $g = 130$  (90% fractional filling). The bunch length and bunch centroid are labeled with BL and BC respectively.

## REFERENCES

[1] G. Bassi, A. Blednykh and V. Smaluk, *Phys. Rev. Accel. Beams* **19**, 024401, 2016.

[2] NSLS-II Conceptual Design Report, 2006.  
 [3] N. Towne, NSLS-II Tech Note 19, 2006; N. Towne, NSLS-II Tech Note 37, 2007; N. Towne, NSLS-II Tech Note 27, 2007; N. Towne, NSLS-II Tech Note 18, 2006.  
 [4] G. Bassi and J. Tagger, NSLS-II Tech Note 286, 2018.  
 [5] G. Penco and M. Svandrik, *Phys. Rev. ST Accel. Beams* **9**, 044401, 2006.  
 [6] M. Predozzi *et al.*, in *Proc. 11th Workshop on RF Superconductivity*, Lübeck/Travemünde, Germany, paper MOP25, 2003.  
 [7] G. Penco, Ph.D. thesis, Sincrotrone Trieste – University of Milan, 2004.  
 [8] R. A. Bosh, K. J. Kleman, and J. J. Bisognano, “Robinson Instabilities with higher-harmonic cavity”, *Phys. Rev. ST Accel. Beams* **4**, 074401, 2001; R. A. Bosh, *Phys. Rev. ST Accel. Beams* **8**, 084401, 2005.  
 [9] A. Hofmann and Myers, in *Proc. 11<sup>th</sup> Int. Conf. on High Energy Accelerators*, Geneva, 1980.  
 [10] K.Y. Ng, “Physics of Intensity Dependent Beam Instabilities”, Fermilab-FN-0713.  
 [11] NERSC, <http://www.nersc.org>  
 [12] G. Bassi and J. Tagger, in preparation.

Content from this work may be used under the terms of the CC BY 3.0 licence (© 2018). Any distribution of this work must maintain attribution to the author(s), title of the work, publisher, and DOI.